J Comput Electron (2017) 16:756–764
DOI 10.1007/s10825-017-0985-8

Manipulation of structural and optical properties in ZnO/ZnS type-II and ZnS/ZnO inverted type-II core/shell nanocrystals: tight-binding theory

Worasak Sukkabot[1]

Published online: 18 April 2017

Abstract Based on the atomistic tight-binding theory (TB), I report here the results of my theoretical investigation into the electronic structures and optical properties of ZnO/ZnS type-II and ZnS/ZnO inverted type-II core/shell nanocrystals, with special emphasis on the single-particle spectra, atomistic orbital characters, optical band gaps, overlaps of ground electron and hole wave functions, ground-state oscillation strengths, electron–hole interactions and Stokes shift under the variation of the coated shell thicknesses. The underlying mechanism from an analysis of the computations is sensitive to the band alignments and growth shell thickness. In the presence of the terminated shell, the optical band gaps of ZnO/ZnS core/shell nanocrystals are reduced, while those of ZnS/ZnO core/shell nanocrystals are increased. With the increasing monolayers of the growth shell, the optical band gaps of ZnO/ZnS and ZnS/ZnO core/shell nanocrystals are decreased because of quantum confinement. It is expected that selecting ZnS as a shell for ZnO nanocrystals, with its large core and growth shell sizes, leads to the formation of the lower band gaps into the visible light spectrum. High optical behaviour is observed in ZnO/ZnS core/shell nanocrystals. As described by electron–hole coulomb interaction, a strong confinement between electrons and holes is found in ZnS/ZnO core/shell nanocrystals. The energies of electron–hole coulomb interaction are reduced with the increasing thickness of the coated shell. The Stokes shift of ZnS/ZnO core/shell nanocrystals is greater than that of ZnO/ZnS core/shell nanocrystals as elucidated by the electron–hole exchange interaction. The reduction of Stokes shift is presented with the increasing passivated shell monolayers. Finally, the present systematic study on the structural and optical properties mainly exposes a new viewpoint to understand the shell-size- and band-profile-dependent behaviours of ZnO/ZnS type-II and ZnS/ZnO inverted type-II core/shell nanoparticles to provide detailed information for use in designing electronic nanodevices.

Keywords Tight-binding theory · ZnO/ZnS · ZnS/ZnO · Coulomb energies · Exchange energies · Stokes shift

1 Introduction

In recent years, semiconductor nanocrystals have attracted much attention because of their unique physical and chemical properties, finding many potential applications in light-emitting diodes [1,2], solar cells [3–6], lasers [7] and biological imaging [8–11]. ZnO is one of the semiconductors with a wide direct band gap, consequently it is a promising material for optical devices such as light emitting diodes and laser diodes [12,13]. Though ZnO is an abundant, stable and environmental material, the band gap of ZnO semiconductors is too large to absorb or emit radiation in the visible region. This may limit the material's optoelectronic applications in the visible spectra. To overcome this restriction, ZnO semiconductors are terminated by a larger band gap of a ZnS shell, making a so-called core/shell nanocrystal. Semiconductor core/shell nanocrystals are composed of two different materials, an interior core and an outer growth shell. By changing the sizes of each region, the physical properties can be manipulated. ZnS is a non-toxic semiconductor with a wide and direct band gap. The coated shell is a physical barrier between the optically active core and the surrounding medium. As a result, type-II band align-

✉ Worasak Sukkabot
w.sukkabot@gmail.com

[1] Department of Physics, Faculty of Science, Ubon Ratchathani University, 85 Sathollmark Rd. Warinchamrab, Ubon Ratchathani 34190, Thailand

ment may contribute to reducing the band gaps into the visible light region. According to the obtained core/shell nanocrystals, one can tune the structural and optical properties of a core/shell nanocrystal by varying the coated shell thicknesses. Therefore, it is important to investigate synthesis methods and theoretical studies that describe the impact of the passivated shell thickness on the physical properties of ZnO/ZnS type-II core/shell nanocrystals. Nam et al. [14] synthesized ZnO/ZnS nanostructures using a thioacetamide (TAA) solution in deionized water. The ZnS shell structure was strongly affected by the concentration of the TAA. The ultraviolet (UV) emission of ZnO/ZnS nanostructure was prominently improved in the comparison with pure ZnO powder. Using the self-consistent charge density-functional tight-binding (SCC-DFTB) method, Saha and Sarkar [15] presented theoretical investigations on the electronic structures of ZnO/ZnS core/shell quantum dots, which were possibly manipulated by terminating the surfaces with different ligands. Implementing a facile one-step method, the synthesis of ZnO/ZnS type-II core/shell nanostructures was reported by Sookhakian et al. [16]. In comparison with ZnO nanoparticles, the photoluminescence emission of ZnO/ZnS core/shell nanostructure was decreased because of the type-II band profile. Sadollahkhani et al. [17] prepared ZnO/ZnS core/shell nanoparticles by the co-precipitation method. The band gap of the ZnO/ZnS core/shell nanocrystal was smaller than that of the ZnO core and ZnS shell materials. Based on the effective-mass approximation, Zeng et al. [18] investigated the linear, nonlinear and total absorption coefficients and refractive index changes associated with intersubband transitions in ZnO/ZnS and ZnS/ZnO core/shell quantum dots under the influence of the shell thickness, impurity and dielectric environment. The computations were mainly affected by these calculated parameters. Based on the literature reviews, there are several experimental works concerned with describing the sizes in the growth shell of ZnO/ZnS core/shell nanocrystals, while theoretical studies describe the SCC-DFTB method and the effective-mass approximation. The atomistic analysis of band alignments remains an open inquiry. Therefore, it is my challenge not only to study the effect of the coated shell thickness but also to determine the band profile on the structural and optical properties of ZnO/ZnS and ZnS/ZnO core/shell nanocrystals with several thousand atoms using the atomistic tight-binding theory. In the present study, ZnO/ZnS and ZnS/ZnO heterostructures display type-II and inverted type-II band profile, respectively. In this manuscript, all investigated core/shell nanocrystals are spherical nanoparticles. This is the aim I aspire to accomplish here.

In order to clarify and analyze the effect of passivated shell thickness and band alignment on the electronic structures and optical properties of ZnO/ZnS and ZnS/ZnO core/shell nanocrystals, I present the single-particle spectra, atomistic orbital characters, optical band gaps, ground electron–hole wave function overlaps, ground-state oscillation strengths, atomistic electron–hole interactions and Stokes shift as a function of the growth shell thicknesses using atomistic tight-binding theory. Because of the high computational demand of the first-principle calculations, the tight-binding model is widely exploited to study the structural and optical properties of large, complicated nanostructures. In the present model, the atomistic tight-binding theory with sp^3 orbitals, I propose to use the first nearest neighboring interaction and spin-orbital coupling. Because of the lattice mismatch between core and shell, the atomic positions additionally have to be optimized by the valence force field method. Finally, the excitonic states and energies are numerically solved by the configuration interaction approach (CI).

To analyze how the growth shell thickness and band profiles influence the structural and optical properties of ZnO/ZnS type-II and ZnS/ZnO inverted type-II core/shell nanocrystals, the organization of the manuscript is as follows. Section 2 gives a brief outline of the theoretical model. Using an effective computational model based on the empirical tight-binding theory, the calculations are mainly discussed in Sect. 3. I emphasize that the atomistic computations are significantly sensitive with the terminated shell thickness and band alignments. The present work is expected to provide information on engineering the natural properties by changing terminated shell thickness and band profiles with the purpose to be implemented in the novel electronic applications. Finally, the resulting computations are summarized in Sect. 4.

2 Theoretical model

For the numerical analysis, a simple but effective computational model based on empirical tight-binding theory is utilized to investigate the electronic structures and optical properties of ZnO/ZnS type-II and ZnS/ZnO inverted type-II core/shell nanoparticles with several thousand atoms and spherical shape. According to the literature [14–17], the studied crystal displays the wurtzite structure generated by a hexagonal closely packed lattice (HCP) with four atoms per unit cell. The surfaces of the core/shell nanocrystals are encapsulated with hydrogen atoms with the intention to avoid the gap states. Because of the heterostructures, the strain field and valence-band offset have to be included into the model. In terms of the strain distribution, the atomistic valence force field (VFF) method is numerically implemented to optimize the relaxed atomic positions as described in more detail in Refs. [19–22]. Two empirical force constants (α and β) [23] are used to define the atomistic valence force field approach. The valence-band offset of +0.84 eV [24], as depicted in Fig. 2, is incorporated into the atomistic model.

Consequently, the sp^3 tight-binding wave functions [25] are generated from one s orbital and three p orbitals (p_x, p_y and p_z) per spin component localized on the sites R in ZnO/ZnS or ZnS/ZnO core/shell nanocrystals, as given by.

$$|R\,\alpha\rangle\,,\ \alpha \in \{s\uparrow, p_x\uparrow, p_y\uparrow, p_z\uparrow, s\downarrow, p_x\downarrow, p_y\downarrow, p_z\downarrow\}.$$

To describe the atomistic tight-binding Hamiltonian (H_{TB}), the particle on the orbital α of atom R under the total number of atoms N is created (annihilated) by the operators $c^{\dagger}_{R\,\alpha}(c_{R\,\alpha})$, respectively.

$$H_{TB} = \sum_{R=1}^{N}\sum_{\alpha=1}^{8} \underset{R\,\alpha}{\varepsilon}\, c^{\dagger}_{R\,\alpha}c_{R\,\alpha} + \sum_{R=1}^{N}\sum_{\alpha=1}^{8}\sum_{\alpha'=1}^{8} \underset{R\,\alpha\,\alpha'}{\lambda}\, c^{\dagger}_{R\,\alpha}c_{R\,\alpha'} + \sum_{R=1}^{N}\sum_{R'=1}^{N}\sum_{\alpha=1}^{8}\sum_{\alpha'=1}^{8} t_{R\,\alpha,R'\,\alpha'}c^{\dagger}_{R\,\alpha}c_{R'\,\alpha'},$$

where $\varepsilon_{R\,\alpha}$, $\lambda_{R\,\alpha\,\alpha'}$ and $t_{R\,\alpha,R'\,\alpha'}$ are the on-site orbital energies, the spin-orbit coupling constant and the hopping matrix elements, respectively. To accurately fit the bulk band structures, the bulk band gaps and the effective masses, I implement the parameterization scheme presented by Kobayashi et al. [26] in Table 1. The parameterization in Table 1 with parameter V is numerically related to parameter t via the Slater–Koster rules [27]. Due to the influence of the strain distribution influenced by the heterostructure, the hopping matrix elements (V) are changed as:

$$V' = V\left(\frac{d_0}{d}\right)^n$$

V and V' are the ideal and strained hopping matrix elements, respectively. d_0 and d are the bond lengths of the unstrained and strained binary semiconductors, respectively.

Table 1 The parameterization scheme of ZnO and ZnS semiconductor. [26]

Parameters	ZnO	ZnS
E(s, a)	−19.046	−10.634
E(p, a)	4.142	1.574
E(s, c)	1.666	2.134
E(p, c)	12.368	6.626
V(s, s)	−6.043	−4.904
V(x, x)	7.157	3.229
V(x, y)	10.578	5.168
V(sa, pc)	4.703	0.357
V(pa, sc)	8.634	6.240
λ_a	0.032	0.025
λ_c	0.085	0.085

In addition, n of 2.0 is defined owing to the principle of Harrison's d^{-2} rule [28]. At the interface between ZnO and ZnS, the atom configuration is Zn–O–Zn–S–Zn. The Zn atoms can bond with either O or S atoms. Hence, the averages of the empirical force constants and tight-binding parameters are treated for the Zn atoms at the heterojunction. To obtain the single-particle states and energies, the large matrix of the atomistic tight-binding Hamiltonian is computationally diagonalized by PReconditioned Iterative MultiMethod Eigensolver (PRIMME) [29,30]. Subsequently, the Hamiltonian of single excitonic states is given by:

$$H = \sum_i E_i\, e_i^{\dagger}\, e_i + \sum_j E_j\, h_j^{\dagger}\, h_j - \sum_{ijkl} V_{ijkl}^{\mathrm{eh,coul}}\, h_i^{\dagger}\, e_j^{\dagger}\, e_k\, h_l + \sum_{ijkl} V_{ijkl}^{\mathrm{eh,exch}}\, h_i^{\dagger}\, e_j^{\dagger}\, e_k\, h_l.$$

The single excitonic Hamiltonian is numerically solved by configuration interaction description (CI) [31–37]. The first two terms stand for the single-particle energies of the ith electron and the jth hole states, respectively. The third and fourth terms arise from the electron–hole coulomb and exchange interaction, respectively. The exchange term is important for the splitting of the excitonic states. Since the single excitonic Hamiltonian is diagonalized, the excitonic energies and states are finally achieved.

3 Results and discussions

As only the first-principle calculation exists in the literature, I intend to analyze the atomistic impact of the band confinement and growth shell thickness on the structural and optical properties of ZnO/ZnS type-II and ZnS/ZnO inverted type-II core/shell nanocrystals with several thousand atoms using the computational model based on the atomistic tight-binding theory (TB) and configuration interaction description (CI). Here, the studied ZnO/ZnS type-II and ZnS/ZnO inverted type-II core/shell nanocrystals are the nanoparticle type with spherical shape. The geometric shape is displayed in Fig. 1 for the selected ZnO/ZnS core/shell nanocrystal with diameter of 3.0 nm and shell thickness of 2.0 monolayers (ML). The potential confinements of ZnO/ZnS and ZnS/ZnO core/shell nanocrystals are displayed in Fig. 2. In the ZnO/ZnS core/shell nanocrystal, the electron is localized within the ZnO core regime but the hole is confined in the ZnS shell region. In the ZnS/ZnO core/shell nanocrystal, the electron is localized in the ZnO shell while the hole is confined in the ZnS core. The increasing layers of growth shell in the range from 0.0 to 5.0 monolayers (ML) are terminated on a core with diameter of 3.00 nm. Using these structural parameters, the single-particle spectra, atomistic characters,

optical band gaps, overlaps of electron and hole wave function, oscillation strengths, electron–hole interactions and Stokes shift are numerically calculated. In the present investigation, the studied sizes of core/shell nanocrystals are much smaller than the experimentally synthesized dimensions, so I have not attempted to present the comparison. However, my theoretical results tend to mainly predict and provide guidelines and the trends to experimentalists operating with inexpensive means. For this purpose, I begin with the single-electron and -hole spectra of ZnO/ZnS and ZnS/ZnO core/shell nanocrystals as a function of the growth shell thicknesses (t_s) in Figs. 3 and 4, respectively. With the appearance of the coated shell, the single-particle spectra of ZnO/ZnS and ZnS/ZnO core/shell nanocrystals are enhanced as compared to the single ZnO and ZnS nanocrystals because of the valence-band offset between core and shell. With the increasing passivated shell, the electron levels of ZnO/ZnS and ZnS/ZnO core/shell nanocrystals are reduced, whereas the hole levels of ZnO/ZnS and ZnS/ZnO core/shell nanocrystals are increased. The single-electron energies of ZnS/ZnO core/shell nanocrystals are greater than those of ZnO/ZnS core/shell nanocrystals, whereas the single-hole energies of ZnO/ZnS core/shell nanocrystals are higher than those of ZnS/ZnO core/shell nanocrystals. These behaviors can be described by the different potential band alignments in both core/shell nanocrystals. Besides, the breaking symmetry is induced by the wurtzite structure of ZnO/ZnS and ZnS/ZnO core/shell nanocrystals, so the degeneracies of the electron states (e_2, e_3 and e_4) and hole states (h_2, h_3 and h_4) are not found. The theoretical analysis of electron and hole character is also reported with the aim of understanding the orbital localization inside the ZnO/ZnS and ZnS/ZnO core/shell nanocrystals. Figure 5 depicts the s-orbital-like character of the ground electron states in the ZnO/ZnS and ZnS/ZnO core/shell nanocrystals. The improvement of the s-orbital-like character is realized in the presence of the coated shell. Nevertheless, there is no change of the s-orbital-like character under the variation of the growth shell thicknesses. Figure 6 demonstrates the heavy-hole-like character of ZnO/ZnS and ZnS/ZnO core/shell nanocrystals with different growth shell thicknesses. The heavy-hole-like characters are enhanced with the inclusion of the terminated shell. The increasing thicknesses of the coated shell does not change the heavy-hole-like characters localized in ZnO/ZnS and ZnS/ZnO core/shell nanocrystals. The band profiles mainly affect the magnitudes of the heavy-hole-like characters, while there is no dependence on the s-orbital-like character. The 2D charge densities of ground electron and hole states of the ZnO nanocrystal and ZnO/ZnS core/shell nanocrystal with t_s of 2.0 ML in the xy plane are displayed in Fig. 7. The electron and hole are mainly confined to the center of the ZnO nanocrystal. In the presence of the ZnS growth shell, the electron is localized within the ZnO core, while the hole is confined in the ZnS shell. Figure 8 demonstrates the 2D charge densities of ground electron and hole states of the ZnS nanocrystal and ZnS/ZnO core/shell nanocrystal with t_s of 2.0 ML spanning in the xy plane. The electron and hole are mainly localized in the center of the ZnS nanocrystal. In the ZnS/ZnO core/shell nanocrystal, electron and hole are localized in the ZnO shell and the ZnS core, respectively. In Fig. 9, I display the variation of the optical gaps of ZnO/ZnS and ZnS/ZnO core/shell nanocrystals as a function of sizes in the growth shell. In the presence of the coated shell, the optical band gaps of ZnO/ZnS core/shell nanocrystals are decreased, while those of the ZnS/ZnO core/shell nanocrystals are promoted. So, ZnO/ZnS core/shell nanocrystals exhibit a red shift in their absorption spectra as compared to bare ZnO nanocrystal. However, ZnS/ZnO core/shell nanocrystals demonstrate a blue shift in the optical spectra in comparison with the single ZnS nanocrystal. The plot clearly reveals that the optical band gaps are progressively reduced with the increasing growth shell thicknesses because of quantum confinement. The red shift in the absorption spectra is displayed with increasing shell thickness. Importantly, the optical band gaps of ZnS/ZnO core/shell nanocrystals are much greater than those of ZnO/ZnS core/shell nanocrystals. It is anticipated that ZnO/ZnS type-II core/shell nanocrystals with thick shells push the band gaps lower into the visible light spectrum. As a result, the optical band gaps are not only manipulated by the growth shell thickness but also by the band profiles, thus providing a new opportunity to fabricate electronic nanodevices.

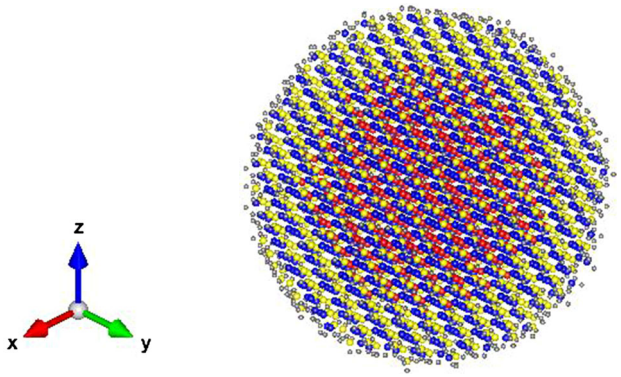

Fig. 1 Schematic of the ZnO/ZnS core/shell nanocrystal with diameter of 3.0 nm and shell thickness of 2.0 monolayers (ML) (*Blue* is Zn, *red* is O, *yellow* is S and *grey* is H) (Color figure online)

The ground electron–hole wave function overlaps ($\langle \Psi^{h=1} | \Psi^{c=1} \rangle$) of ZnO/ZnS and ZnS/ZnO core/shell nanocrystals as a function of the growth shell thicknesses as illustrated in Fig. 10. The aim is to theoretically understand the localization of the carriers under different band alignments and growth shell thicknesses. It is noticeable that the growth shells substantially reduce the ground electron–hole wave function overlaps due to the spatial electron–hole wave function

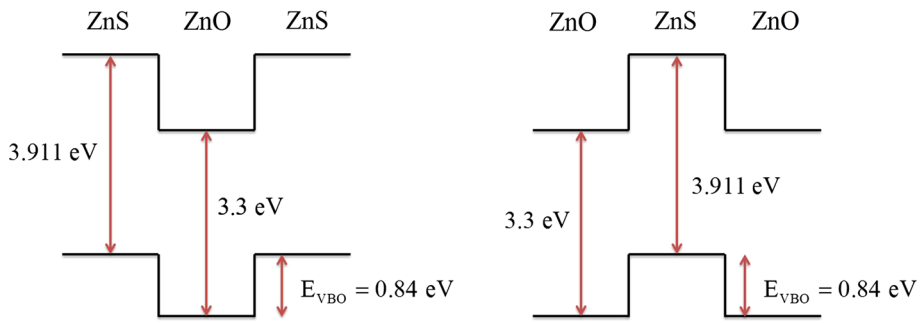

Fig. 2 Band profiles of ZnO/ZnS type-II and ZnS/ZnO inverted type-II core/shell nanocrystals, VBO = Valence-Band Offset

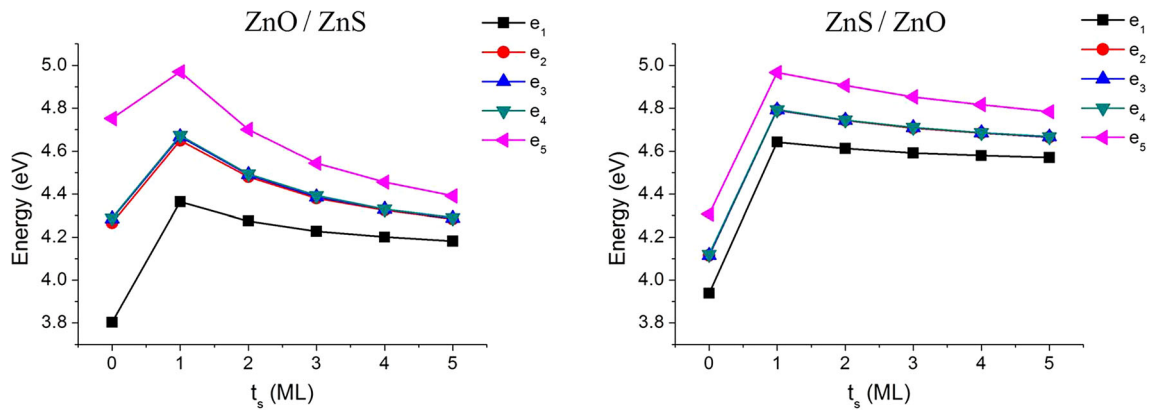

Fig. 3 Single-electron energies of ZnO/ZnS type-II and ZnS/ZnO inverted type-II core/shell nanocrystals as a function of growth shell thicknesses (t_s). e_i is the ith electron state

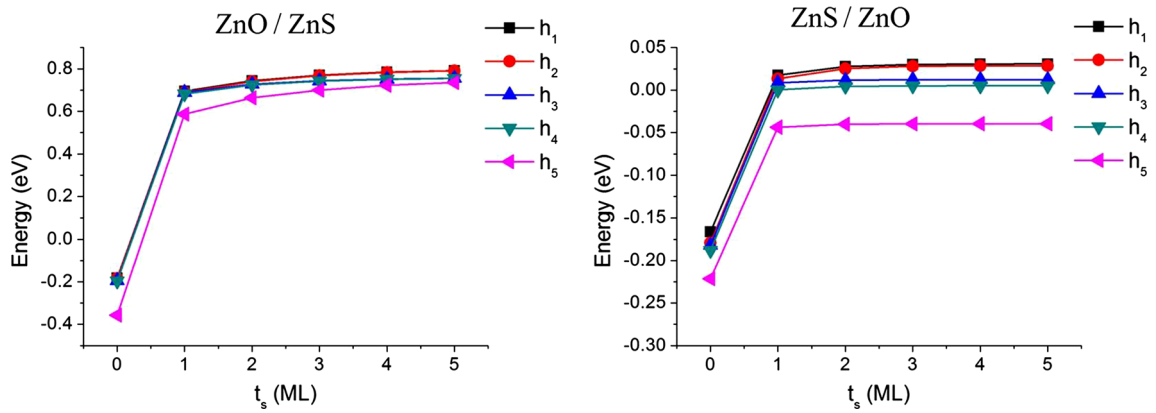

Fig. 4 Single-hole energies of ZnO/ZnS type-II and ZnS/ZnO inverted type-II core/shell nanocrystals as a function of growth shell thicknesses (t_s). h_i is the ith hole state

localization. The electron and hole are confined in different regimes in the presence of the coated shell as demonstrated by the band profiles in Fig. 2. As can be seen, the ground electron–hole wave function overlaps are unaffected by the sizes in the terminated shell. A comparison of the band profiles shows that the ground electron–hole wave function overlaps of the ZnS/ZnO core/shell nanocrystals are greater than those of the ZnO/ZnS core/shell nanocrystals. To observe the optical properties, I show the ground-state oscillation strengths of ZnO/ZnS and ZnS/ZnO core/shell nanocrysyals as illustrated in Fig. 11. The oscillation strengths (f_{ij}) between electron (i) and hole (j) states are calculated via this equation $f_{ij} = \frac{2m_0}{\hbar^2}\left|\hat{e}\cdot\vec{D}_{ij}\right|^2 \times \left(E_i - E_j\right)$, with m_0, E_i and E_j being the free-electron mass, the energies of electron (i) and hole (j) states, respectively. $\vec{D}_{ij}$ are the dipole moments of the inter-band transitions between electron (i) and hole (j) states. In the present calculations, I consider the polarized vector ($\hat{e}$) in the xy plane [110]. In comparison with the single nanocrystals, the terminated shells significantly induce the reduction of ground-state oscillation strengths, thus leading

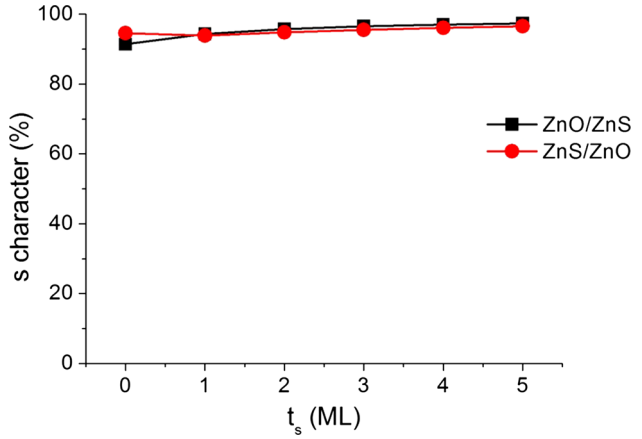

Fig. 5 *s* orbital-like character of ZnO/ZnS type-II and ZnS/ZnO inverted type-II core/shell nanocrystals as a function of growth shell thicknesses (t_s)

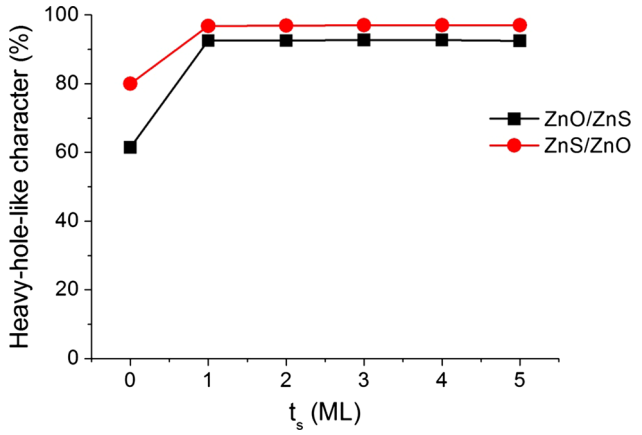

Fig. 6 Heavy-hole-like character of ZnO/ZnS type-II and ZnS/ZnO inverted type-II core/shell nanocrystals as a function of growth shell thicknesses (t_s)

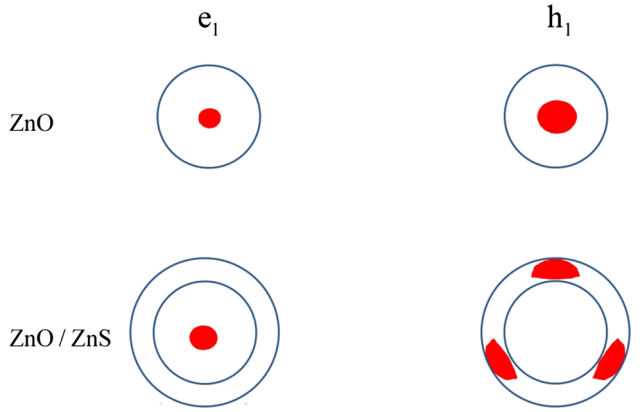

Fig. 7 2D charge densities of ground electron (e_1) and hole (h_1) states of ZnO nanocrystal and ZnO/ZnS core/shell nanocrystal with t_s of 2.0 ML

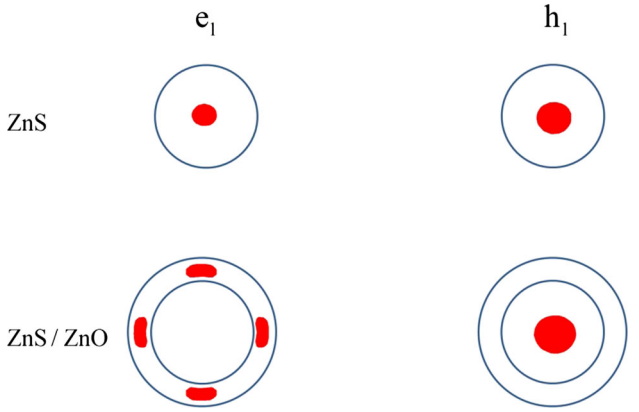

Fig. 8 2D charge densities of ground electron (e_1) and hole (h_1) states of ZnS nanocrystal and ZnS/ZnO core/shell nanocrystal with t_s of 2.0 ML

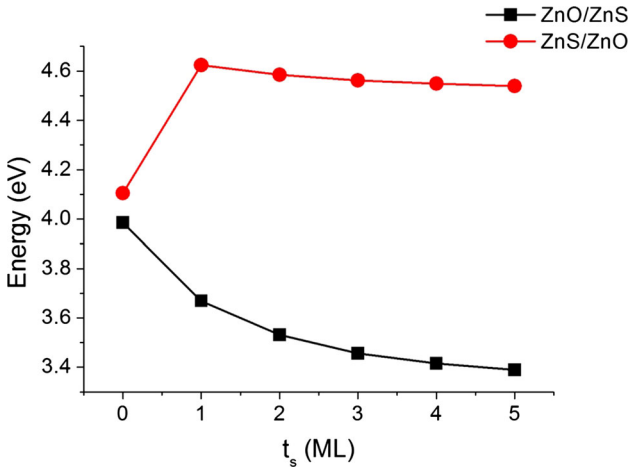

Fig. 9 Optical band gaps of ZnO/ZnS type-II and ZnS/ZnO inverted type-II core/shell nanocrystals as a function of growth shell thicknesses (t_s)

to the lower optical properties in core/shell nanocrystals. This observation is consistent with previous experimental studies [14,16]. The oscillation strengths are steadily decreased as the coated shell thickness is sequentially increased, indicating poorer optical performance in a thick shell. A close look at the figure reveals that the optical property of a ZnS shell coated on a ZnO core is better than that of a ZnO shell terminated on a ZnS core. Therefore, the optical behaviour is handled by changing the band profiles and passivated shell thickness, whereas the better optical properties are obviously observed in the single nanocrystals.

The atomistic electron–hole interactions are analyzed by means of coulomb and exchange terms. The electron–hole coulomb interaction describes the bound state between electron and hole localized in the studied core/shell nanocrystals. The Stokes shift is elucidated by the exchange interaction between electron and hole. Figures 12 and 13 present the ground electron–hole coulomb and exchange energies of ZnO/ZnS and ZnS/ZnO core/shell nanocrystals under different growth shell thicknesses, respectively. From the figures, it is clear that the fragile atomistic electron–hole interac-

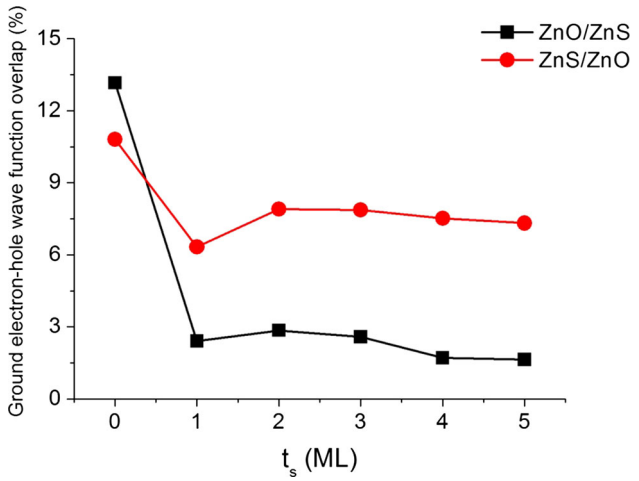

Fig. 10 Ground electron–hole wave function overlaps of ZnO/ZnS type-II and ZnS/ZnO inverted type-II core/shell nanocrystals as a function of growth shell thicknesses (t_s)

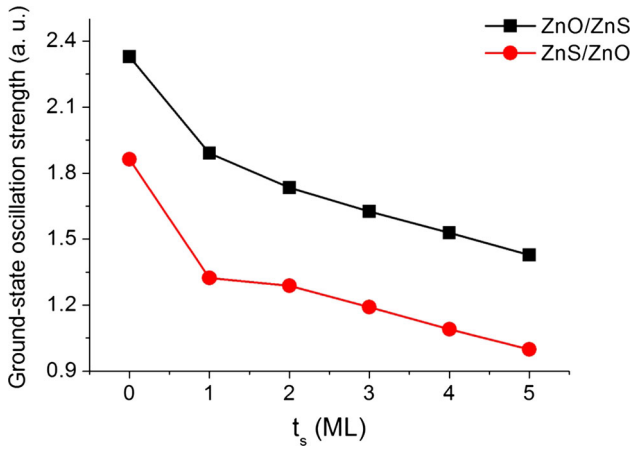

Fig. 11 Ground-state oscillation strengths of ZnO/ZnS type-II and ZnS/ZnO inverted type-II core/shell nanocrystals as a function of growth shell thicknesses (t_s)

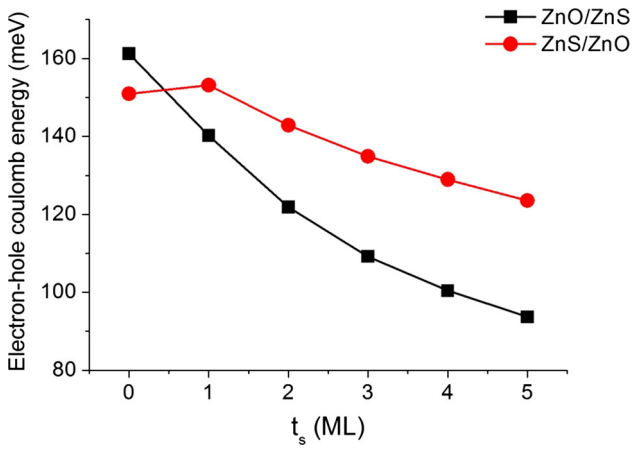

Fig. 12 Electron–hole coulomb energies of ZnO/ZnS type-II and ZnS/ZnO inverted type-II core/shell nanocrystals as a function of growth shell thicknesses (t_s)

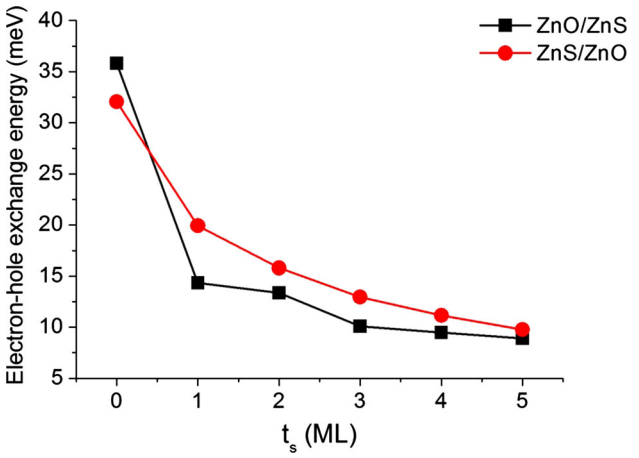

Fig. 13 Electron–hole exchange energies of ZnO/ZnS type-II and ZnS/ZnO inverted type-II core/shell nanocrystals as a function of growth shell thicknesses (t_s)

tions are steadily realized with the increasing passivated shell thicknesses. The electron–hole bound state and Stokes shift are mainly reduced with the increasing growth shell thicknesses. In terms of the band profiles, the atomistic electron–hole interactions of ZnO nanocrystal are initially greater than those of ZnS nanocrystal. However, in the presence of the coated shell, the electron–hole interactions of ZnS/ZnO core/shell nanocrystals are stronger than those of ZnO/ZnS core/shell nanocrystals. The electron and hole tend to be more localized in ZnS/ZnO core/shell nanocrystals than in ZnO/ZnS core/shell nanocrystals. It is expected that the Stokes shift of ZnS/ZnO core/shell nanocrystals is greater than that of ZnO/ZnS core/shell nanocrystals. Therefore, the atomistic electron–hole coulomb and exchange interactions can be controlled by the size of the growth shell and the potential confinements.

Finally, I try to shed some light on the Stokes shift of ZnO/ZnS and ZnS/ZnO core/shell nanocrystals under different monolayers of the growth shell in Fig. 14. The Stokes shift is the energy difference between the lowest optically forbidden excitonic state and the lowest optically allowed excitonic state. In the present manuscript, the lowest excitonic states of ZnO/ZnS and ZnS/ZnO core/shell nanocrystals are prepared from the twofold highest valence levels and the twofold lowest conduction levels in the presence of the spin components. Using the configuration interaction description (CI) in the conjunction with 12 electron and hole levels, the electron–hole coulomb and exchange interaction computationally split the fourfold state into a two-fold degenerate lower (dark) state and a two-fold degenerate upper (bright) state. With increasing terminated shell thicknesses, the Stokes shift of ZnO/ZnS and ZnS/ZnO core/shell nanocrystals is progressively reduced as described by the trend of the electron–hole exchange interaction. In terms of the band profiles, the

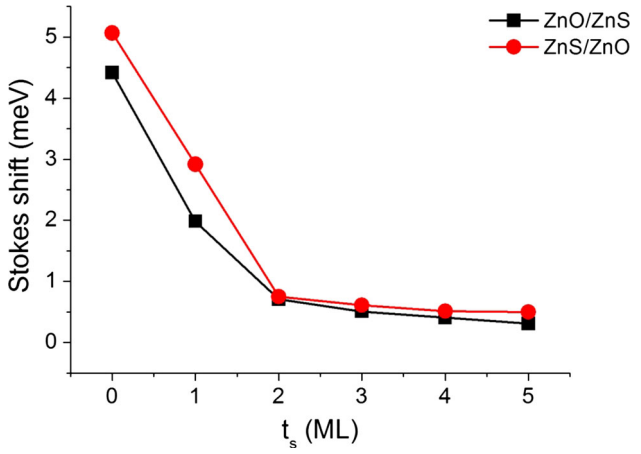

Fig. 14 Stokes shift of ZnO/ZnS type-II and ZnS/ZnO inverted type-II core/shell nanocrystals as a function of growth shell thicknesses (t_s)

Stokes shifts of ZnS/ZnO core/shell nanocrystals are greater than those of ZnO/ZnS core/shell nanocrystals because the exchange energies between electron and hole in ZnS/ZnO core/shell nanocrystals are higher than those in ZnO/ZnS core/shell nanocrystals. This suggests the possibility of tailoring the Stokes shift by changes in band alignments and passivated shell thicknesses.

4 Conclusions

In the present manuscript, I theoretically study the electronic structures and optical properties of ZnO/ZnS type-II and ZnS/ZnO inverted type-II core/shell nanoparticles with several thousand atoms and spherical shape as a function of the growth shell thicknesses by means of the empirical tight-binding framework (TB) and configuration interaction description (CI). The changes in band profiles and encapsulated shell thicknesses predominantly lead to a strong effect of correlation on the structural and optical properties. With increasing sizes of the growth shell, a reduction of the optical band gaps is evident because of quantum confinement. The optical band gaps of ZnS/ZnO core/shell nanocrystals are greater than those of ZnO/ZnS core/shell nanocrystals. I predict that ZnO/ZnS type-II core/shell nanocrystals with thick shells and massive cores are primarily propelled to lower the optical band gaps into the visible light regions. The optical properties are mainly lower with increasing coated shell thicknesses. The optical properties of ZnO/ZnS core/shell nanocrystal are higher than those of ZnS/ZnO core/shell nanocrystal. The weak atomistic electron–hole interactions are steadily realized with the increasing passivated shell thicknesses. In terms of the band profiles, the atomistic electron–hole interactions of ZnO nanocrystals are greater than those of ZnS nanocrystals. In the presence of a coated shell, the strong electron–hole interactions are observed in ZnS/ZnO core/shell nanocrystals. In addition, the Stokes shift of ZnO/ZnS and ZnS/ZnO core/shell nanocrystals is progressively decreased with the increasing terminated shell thicknesses. The pronounced Stokes shift is mainly probed in ZnS/ZnO core/shell nanocrystals. The manipulation of the electronic structures and optical properties in ZnO/ZnS type-II and ZnS/ZnO inverted type-II core/shell nanocrystals is finally performed by changing the terminated shell thicknesses and confinement potentials with the purpose of implementing them in the desirable nanoelectronic applications.

Acknowledgements The author would like to acknowledge the financial support from the Thailand Research Fund Grants (TRG58880072) and kindly support from Department of Physics, Faculty of Science, Ubon Ratchathani University, Thailand.

References

1. Bowers, M.J., McBride, J.R., Rosenthal, S.J.: White-light emission from magic-sized cadmium selenide nanocrystals. J. Am. Chem. Soc. **127**, 15378–15379 (2005)
2. Anikeeva, P.O., Madigan, C.F., Coe-Sullivan, S.A., Steckel, J.S., Bawnendi, M.G., Bulovic, V.: Photoluminescence of CdSe/ZnS core/shell quantum dots enhanced by energy transfer from a phosphorescent donor. Chem. Phys. Lett. **424**, 120–125 (2006)
3. Nozik, A.J.: Quantum dot solar cells. Phys. E **14**, 115–120 (2002)
4. Gur, I., Fromer, N.A., Geier, M.L., Alivisatos, A.P.: Air-stable all-inorganic nanocrystal solar cells processed from solution. Science **310**, 462–465 (2005)
5. Hanna, M.C., Nozik, A.J.: Solar conversion efficiency of photovoltaic and photoelectrolysis cells with carrier multiplication absorbers. J. Appl. Phys. **100**, 074510–074518 (2006)
6. Kamat, P.V.: Quantum dot solar cells. Semiconductor nanocrystals as light harvesters. J. Phys. Chem. C **112**, 18737–18753 (2008)
7. Klimov, V.I., Mikhailovsky, A.A., Xu, S., Malko, A., Hollingsworth, J.A., Leatherdale, C.A., Eisler, H.J., Bawendi, M.G.: Optical gain and stimulated emission in nanocrystal quantum dots. Science **290**, 314–317 (2000)
8. Achilefu, S.: Lighting up tumors with receptor-specific optical molecular probes. Technol. Cancer Res. Treat. **3**, 393–409 (2004)
9. Bruchez, M., Moronne, M., Gin, P., Weiss, S., Alivisatos, A.P.: Semiconductor nanocrystals as fluorescent biological labels. Science **281**, 2013–2016 (1998)
10. Mukherjee, A., Ghosh, S.: Optimum excitation photon energy for CdSe-ZnS core-shell quantum dot based luminescence imaging. J. Phys. D Appl. Phys. **45**, 195103–195107 (2012)
11. Dahan, M., Levi, S., Luccardini, C., et al.: Diffusion dynamics of glycine receptors revealed by single-quantum dot tracking. Science **302**, 442–445 (2003)
12. Mallika, A.N., Ramachandra Reddy, A., Sowri Babu, K., Venugopal Reddy, K.: Synthesis and optical characterization of aluminum doped ZnO nanoparticles. Ceram. Int. **40**, 12171–12177 (2014)
13. Willander, M., Nur, O., Zhao, Q.X., Yang, L.L., Lorenz, M., Cao, B.Q., et al.: Zinc oxide nanorod based photonic devices: recent progress in growth, light emitting diodes and lasers. Nanotechnology **20**, 1–40 (2009)

14. Nam, W.H., Lim, Y.S., Seo, W.-S., Cho, H.K., Lee, J.Y.: Control of the shell structure of ZnO-ZnS core-shell structure. Nanopart. Res. **13**, 5825–5831 (2011)
15. Saha, S., Sarkar, P.: Electronic structure of ZnO/ZnS core/shell quantum dots. Chem. Phys. Lett. **555**, 191–195 (2013)
16. Sookhakian, M., Amin, Y.M., Basirun, W.J., Tajabadi, M.T., Kamarulzaman, N.: Synthesis, structural, and optical properties of type-II ZnO-ZnS core-shell nanostructure. J. Lumin. **145**, 244–252 (2014)
17. Sadollahkhani, A., Nur, O., Willander, M., Kazeminezhad, I., Khranovskyy, V., Eriksson, M.O., Yakimova, R., Holtz, P.-O.: "A detailed optical investigation of ZnO@ZnS core-shell nanoparticles and their photocatalytic activity at different pH values". Ceram. Int. **41**, 7174–7184 (2015)
18. Zeng, Z., Garoufalis, C.S., Terzis, A.F., Baskoutas, S.: Linear and nonlinear optical properties of ZnO/ZnS and ZnS/ZnO core shell quantum dots: effects of shell thickness, impurity, and dielectric environment. J. Appl. Phys. **114**, 023510–023519 (2013)
19. Keating, P.N.: Effect of invariance requirements on the elastic strain energy of crystals with application to the diamond structure. Phys. Rev. **145**, 637–645 (1966)
20. Martin, R.M.: Elastic properties of ZnS structure semiconductors. Phys. Rev. B **1**, 4005–4011 (1970)
21. Sukkabot, W.: Variation in the structural and optical properties of CdSe/ZnS core/shell nanocrystals with ratios between core and shell radius. Phys. B **454**, 23–30 (2014)
22. Sukkabot, W.: Electronic structure and optical properties of colloidal InAs/InP core/shell nanocrystals: tight-binding calculations. Phys. E Low Dimens. Syst. Nanostruct. **63**, 235–240 (2014)
23. Yadav, D.S., Kumar, C.: Structural properties of binary semiconductors. Int. J. Phys. Sci. **8**(21), 1174–1178 (2013)
24. Schrier, J., Demchenko, D.O., Wang, L., Paul Alivisatos, A.: Optical properties of ZnO/ZnS and ZnO/ZnTe heterostructures for photovoltaic applications. Nano Lett. **7**(8), 2377–2382 (2007)
25. Vogl, P., Hjalmarson, H.P., Dow, J.D.: A Semi-empirical tight-binding theory of the electronic structure of semiconductors. J. Phys. Chem. Solids **44**, 365–378 (1983)
26. Kobayashi, A., Sankey, O.F., Volz, S.M., Dow, J.D.: Semiempirical tight-binding band structures of wurtzite semiconductors: AlN, CdS, CdSe, ZnS, and ZnO. Phys. Rev. B **28**, 935–945 (1983)
27. Slater, J.C., Koster, G.F.: Simplified LCAO method for the periodic potential problem. Phys. Rev. **94**, 1498–1524 (1954)
28. Harrison, A.W.: Elementary Electronic Structure. World Scientific Publishing Company, Singapore (1999)
29. Stathopoulos, A., McCombs, J.R.: PRIMME: preconditioned Iterative multimethod eigensolver: methods and software description. ACM Trans. Math. Softw. **37**(2), 21:1–21:30 (2010)
30. Wu, L., Romero, E., Stathopoulos, A.: PRIMME_SVDS: A High-Performance Preconditioned SVD Solver for Accurate Large-Scale Computations. arXiv:1607.01404
31. Bryant, G.W., Zieliński, M., Malkova, N., Sims, J., Jaskólski, W., Aizpurua, J.: Effect of mechanical strain on the optical properties of quantum dots: controlling exciton shape, orientation, and phase with a mechanical strain. Phys. Rev. Lett. **105**, 067404–067407 (2010)
32. Korkusinski, M., Hawrylak, P.: Atomistic theory of emission from dark excitons in self-assembled quantum dots. Phys. Rev. B **87**, 115310–115320 (2013)
33. Zieliński, M.: Valence band offset, strain and shape effects on confined states in self-assembled InAs/InP and InAs/GaAs quantum dots. J. Phys. Condens. Matter **25**, 465301–465316 (2013)
34. Luo, J.W., Franceschetti, A., Zunger, A.: Nonmonotonic size dependence of the dark/bright exciton splitting in GaAs nanocrystals. Phys. Rev. B **79**, 201301(R)–201304(R) (2009)
35. Bester, G., Nair, S., Zunger, A.: Pseudopotential calculation of the excitonic fine structure of million-atom self-assembled $In_{1-x}Ga_xAs$/GaAs quantum dots. Phys. Rev. B **67**, 161306(R)–161309(R) (2003)
36. Reboredo, F.A., Franceschetti, A., Zunger, A.: Dark excitons due to direct Coulomb interactions in silicon quantum dots. Phys. Rev. B. **61**, 13073–13087 (2000)
37. De Oliveira, E.L., Albuquerque, E.L., De Sousa, J.S., Farias, G.A., Peeters, F.M.: Configuration-interaction excitonic absorption in small Si/Ge and Ge/Si core/shell nanocrystals. J. Phys. Chem. C **116**, 4399–4407 (2012)